Hydrogenation of CO_2 to Methanol on CeO_x/Cu(111) and ZnO/Cu(111) Catalysts: Role of the Metal-Oxide Interface and Importance of Ce^{3+} Sites

Sanjaya D. Senanayake,[1] Pedro J. Ramírez,[2] Iradwikanari Waluyo,[1] Shankhamala Kundu,[1] Kumudu Mudiyanselage,[1] Zongyuan Liu,[1,3] Zhi Liu,[4] Stephanus Axnanda,[4] Dario J. Stacchiola,[1] Jaime Evans,[2] and José A. Rodriguez[1,3]*

[1] Chemistry Department, Department, Brookhaven National Laboratory, Upton, NY 11973, USA

[2] Facultad de Ciencias, Universidad Central de Venezuela, Caracas 1020-A, Venezuela

[3] Department of Chemistry, SUNY Stony Brook, Stony Brook, NY 11790, USA

[4] The Advanced Light Source, Lawrence Berkeley National Laboratory, Berkeley, CA 94720, USA

*Corresponding Author: rodrigez@bnl.gov

ABSTRACT

The role of the interface between a metal and oxide (CeO_x-Cu and ZnO-Cu) is critical to the production of methanol through the hydrogenation of CO_2 ($CO_2+3H_2 \rightarrow CH_3OH + H_2O$). The deposition of nanoparticles of CeO_x or ZnO on Cu(111), $\theta_{oxi} < 0.3$ monolayer, produces highly active catalysts for methanol synthesis. The catalytic activity of these systems increases in the sequence: Cu(111) < ZnO/Cu(111) < CeO_x/Cu(111). The apparent activation energy for the $CO_2 \rightarrow CH_3OH$ conversion decreases from 25 kcal/mol on Cu(111) to 16 kcal/mol on ZnO/Cu(111) and 13 kcal/mol on CeO_x/Cu(111). The surface chemistry of the highly active CeO_x-Cu(111) interface was investigated using ambient pressure X-ray photoemission spectroscopy (AP-XPS) and infrared reflection absorption spectroscopy (AP-IRRAS). Both techniques point to the formation of formates ($HCOO^-$) and carboxylates ($CO_2^{\delta-}$) during the reaction. Our results show an active state of the catalyst rich in Ce^{3+} sites which stabilize a $CO_2^{\delta-}$ species that is an essential intermediate for the production of methanol. The inverse oxide/metal configuration favors strong metal-oxide interactions and makes possible reaction channels not seen in conventional metal/oxide catalysts.

INTRODUCTION

Nowadays there is strong interest in optimizing the configuration of metal-oxide catalysts used for the binding, activation and conversion into valuable chemicals of CO_2. The increasing levels of CO_2 in the atmosphere and oceans are a serious concern for the future of life on our planet.[1] A consequence of this are the strict legal limits on commercial and industrial emissions aimed at mitigating the detrimental effects of CO_2 and other greenhouse pollutants on the environment and climate.[1,2] As a result there are major economic incentives to minimize the production of CO_2 and for methods to capture and sequester/store this molecule.[1,3] In addition, the supply of emitted CO_2 can be used as a new source of fuel, provided that the conversion to a valued commodity such as synthesis gas ($CO + H_2$), oxygenates (alcohols, ethers, acids) or hydrocarbons (CH_4, olefins) is feasible and economical.[4-7] Many research groups are now attempting to activate the CO_2 in the air to produce liquid fuels through hydrogenation using different configurations of metal-oxide catalysts.[3,4,8-12]

There is a resurgence in the study of the hydrogenation of CO_2 to C1 and greater alcohols ($xCO_2 + yH_2 \rightarrow C_xH_3OH + xH_2O$).[6-10,13,14] This process is a classical prototype reaction in both homogenous and heterogeneous catalysis with studies in the literature going back to the 1940's. Today this reaction is predominantly associated with supported Cu based catalysts with a $Cu/ZnO/Al_2O_3$ formulation.[9,14-15] Cu on its own is a poor catalyst for the $CO_2 \rightarrow CH_3OH$ conversion and has a low propensity to do several key steps that lead to CO_2 activation.[10,16-21] An enhancement in the catalytic activity of Cu is frequently observed after dispersing this metal on a ZnO substrate to generate a catalyst with a metal/oxide configuration.[12,15,17,22] However, recent works using high-resolution transmission electron microscopy (HRTEM) have observed the presence of ZnO_x aggregates on top of the copper particles typical of a Cu/ZnO catalyst active for methanol synthesis.[11,14,22] Furthermore, the deposition of ZnO_x nanostructures on polycrystalline copper produces a system with a catalytic activity six times larger than that of plain copper.[16] Synergistic effects between Cu and ZnO_x could be responsible for the catalytic activity of Cu-ZnO.[11,14,16]

Last year our group reported a substantial enhancement in the catalytic activity of Cu(111) after depositing ~ 0.2 ML of CeO_x nanoparticles.[23] The presence of adsorbed $CO_2^{\delta-}$ on the catalyst surface was identified through a combination of ambient-pressure X-ray photoelectron spectroscopy (AP-XPS) and infrared reflection absorption spectroscopy (AP-IRRAS).[23] In this work, we report a comparative study of the catalytic activity of ZnO/Cu(111) and CeO_x/Cu(111) changing in a systematic way the coverage of the oxides on the copper surface. The oxide coverage has a drastic effect on the catalytic activity but in general these inverse catalysts with an oxide/metal configuration are more active than catalysts with standard Cu/ZnO and Cu/CeO_2 configurations. CeO_x/Cu(111) is the most active catalyst. The ceria-copper interface is essential for the binding and transformation of CO_2. Our AP-XPS and AP-IRRAS results show an active state of the catalyst which is rich in Ce^{3+} sites that stabilize $CO_2^{\delta-}$ intermediates involved in the production of methanol.

EXPERIMENTAL SECTION

The catalyst systems were studied in a set-up that combines a ultra-high Vacuum (UHV) chamber for surface characterization (base pressure ~5×10^{-10} Torr) and a batch reactor for catalytic tests.[17,23] The sample could be transferred between the reactor and the UHV chamber without exposure to air. The UHV chamber was equipped with instrumentation for XPS, ultraviolet photoelectron spectroscopy (UPS), low-energy electron diffraction (LEED), ion-scattering spectroscopy (ISS), and thermal-desorption mass spectroscopy (TDS).[17,23] In the studies of CO_2 hydrogenation, the sample was transferred to the reactor at ~ 300 K, then the reactant gases, 0.049 MPa (0.5 atm) of CO_2 and 0.441 MPa (4.5 atm) of H_2, were introduced and the sample was rapidly heated to the reaction temperature (500, 525, 550, 575 and 600 K).[17,23] Product yields were analyzed by a mass spectrometer and/or a gas chromatograph.[18] The amount of molecules (CO or CH_3OH) produced in the catalytic tests was normalized by the active area exposed by the sample and the total reaction time. In the present experiments, data were collected at intervals of 15 min up to total reaction times of 270 min. The kinetic experiments were done in the limit of low conversion (< 5%).

All Ambient Pressure X-ray Photoemission Spectroscopy (AP-XPS) measurements were conducted at the Advanced Light Source (ALS) at Lawrence Berkeley National Laboratory (LBNL) on beamline 9.3.2. The sample preparation was performed in a preparation chamber connected to the analysis chamber. The analysis chamber is equipped with a VG Scienta R4000 HiPP ambient pressure XPS Analyzer and soft X-rays are introduced by way of a Si_3N_4 window. The full description of the beamline, beam characteristics and end station configuration can be found elsewhere.[24] The C 1s, Cu 3s, and Ce 4d regions were collected with a photon energy of 490 eV, while the O 1s region was probed with a photon energy of 700 eV, and a resolution of 0.2–0.3 eV. Energy calibration was performed with the Cu 3s and Ce 4d satellite features. IRRAS experiments were performed in a combined UHV surface analysis chamber and ambient pressure (AP) reactor/IRRAS cell system described elsewhere.[25]

The preparation of the ZnO/Cu(111) and CeO_x/Cu(111) model catalysts was performed by the deposition of zinc or cerium metal in an ambient of O_2 (5×10^{-7}Torr) onto a clean Cu(111) crystal at 600 K. This led to the formation of ZnO/CuO_x/Cu(111) and CeO_2/CuO_x/Cu(111) surfaces which transformed into ZnO/Cu(111) and CeO_x/Cu(111) after exposure to molecular hydrogen.[23] Studies with scanning tunneling microscopy examining the reduction of CeO_2/CuO_x/Cu(111) in molecular hydrogen showed the disappearance of the surface regions of CuO_x and some changes in the morphology of the ceria islands which exhibited internal holes that expose copper-ceria interfaces.[23] When this surface was exposed to a reactant mixture of CO_2/H_2, carbonates formed on the oxide nanoparticles without big changes in morphology. ISS and XPS were used to determine the coverage of ZnO and CeO_x on the copper substrate after reducing the ZnO/CuO_x/Cu(111) and CeO_2/CuO_x/Cu(111) systems with hydrogen. The Cu(111) crystal was cleaned by repeated sputter (1kV, 300 K) and anneal (900 K) cycles.

RESULTS AND DISCUSSION

The hydrogenation of CO_2 on the ZnO/Cu(111) and CeO_x/Cu(111) catalysts produced CO through the reverse water-gas shift reaction ($CO_2 + H_2 \rightarrow H_2O + CO$), methanol and some traces of ethanol ($xCO_2 + yH_2 \rightarrow C_xH_3OH + xH_2O$). As seen in another studies,[12,16,16-20] the rate for the production of CO was 2-3 orders of magnitude larger than the rate for the synthesis of methanol. Figure 1 shows the variation in the rate for methanol synthesis on ZnO/Cu(111) and CeO_x/Cu(111) catalysts as a function of oxide coverage. Under the conditions in which the experiments in Figure 1 were done (T= 550 K, P_{CO2}= 0.5 atm, P_{H2}= 9.5 atm), the rate measured for methanol formation on clean Cu(111) was 0.003 x 10^{15} molecules cm^{-2} s^{-1}. A substantial increase in catalytic activity was observed after the deposition of ZnO and CeO_x on the copper substrate. In both cases, the catalytic activity raised after the deposition of the oxide, reached a maximum and then decreased. In the case of ZnO/Cu(111), the maximum in the rate of methanol formation was seen after covering ~ 20% of the Cu(111) surface with ZnO, very similar to the behavior seen upon deposition of this oxide on polycrystalline copper.[16] For CeOx/Cu(111), the maximum in catalytic activity occurred when the Cu(111) surface was covered 30-40% by ceria. The data in Figure 1 indicate that CeO_x is a better promoter of catalytic activity than ZnO. Since all the catalytic activity disappears after completely covering the Cu(111) substrate, it is clear that the $CO_2 \rightarrow CH_3OH$ conversion was taken place at the Cu-CeO_x and Cu-ZnO interfaces.

Figure 2A displays Arrhenius plots for the synthesis of methanol on clean Cu(111) and on this surface covered ~ 20% by either ZnO or CeO_x. In the range of temperatures investigated (500-600 K), CeO_x/Cu(111) is the best catalyst for the conversion of CO_2 to CH_3OH. The apparent activation energy for the reaction decreases from 25 kcal/mol on Cu(111) to 16 kcal/mol on ZnO/Cu(111) and to 13 kcal/mol on CeO_x/Cu(111). Similar experiments were done for a Cu(111) substrate covered ~ 50 % with ZnO or CeO_x obtaining apparent activation energies of 21 kcal/mol for ZnO/Cu(111) and 14 kcal/mol for CeO_x/Cu(111), see Figure 2B. Again CeO_x/Cu(111) was always the best catalyst.

A comparison of the catalytic activity seen in Figures 1 and 2 for ZnO/Cu(111) with that reported for the Cu/ZnO(000$\bar{1}$) system in the literature[17] indicates that the oxide/metal configuration is by far a superior catalyst, Figure 3. Thus, it is not surprising that this is the active configuration in the industrial Cu/ZnO/Al_2O_3 powder catalyst.[11,14] A similar comparison for the CeO_x/Cu(111) and Cu/CeO_2(111)[23] systems again gives the oxide/metal configuration as the much better catalyst, Figure 3. The deposition of nanoparticles of an oxide on a metal usually produces stronger metal-oxide interactions than observed after depositing nanoparticles of a metal on a bulk oxide due to the intrinsically low reactivity of bulk oxides where even wetting of many metals is problematic.[26,27] The strong bonding existing in oxide/metal configurations can also lead to perturbations or modifications in the electronic properties of the oxide giving novel chemical properties.[28,29]

The chemical state of the surface of the catalysts after reaction was examined with XPS. The as-prepared $ZnO/CuO_x/Cu(111)$ systems transformed into ZnO/Cu(111). Figure 4 shows typical Zn $2p_{3/2}$ XPS spectra and the measured peak position for each catalyst investigated is shown in Figure 5. At the ZnO coverage of maximum activity, ~ 0.2 of Cu(111) covered in Figure 1, a Zn $2p_{3/2}$ peak position near 1021.6 eV was observed. This value is very close to the position of 1021.6-1021.7 eV seen for Zn^{2+} and different from the binding energy of 1021.1 eV observed for Zn^0.[16,30,31] A ZnO/Cu active phase has also been seen after performing the hydrogenation of CO_2 on a Zn/Cu alloy generated by depositing Zn on polycrystalline copper.[16] The oxygen released by the $CO_{2,ads} \rightarrow CO_{ads} + O_{ads}$ reaction probably oxidized the Zn precursor to ZnO.[16] In Figure 5, the Zn $2p_{3/2}$ peak position decreases slightly when the coverage of zinc oxide increases, but it is always close to the values reported for Zn^{2+}.[16,30,31] For a large coverage of zinc oxide, some oxygen vacancies maybe generated inside the oxide film that covers Cu(111) by reaction with hydrogen to form water.

The synthesized $CeO_2/CuO_x/Cu(111)$ surfaces were rapidly reduced to $CeO_x/Cu(111)$ when exposed to H_2 or a CO_2/H_2 reactant mixture. CeO_2 and Ce_2O_3 have quite different line-shapes in the Ce 3d XPS region.[32,33] Ce 3d spectra can be deconvoluted to extract the amount of Ce^{3+} and Ce^{4+} in a ceria sample.[32,33] Figure 6 shows Ce 3d spectra recorded after performing the hydrogenation of CO_2 on a Cu(111) substrate partially or fully covered with ceria. For the small coverage of ceria, the line shape in the Ce 3d region denotes the presence of Ce_2O_3 on the surface of the catalyst.[32,33] On the other hand, the Ce 3d line shape for a surface fully covered with ceria is that of CeO_2.[32,33] Figure 7 displays the measured amount of Ce^{3+} in the

$CeO_x/Cu(111)$ catalysts after reaction. At small coverages of ceria the active phase was essentially $Ce_2O_3/Cu(111)$ as the Ce^{4+} cations in these systems were not stable under a CO_2/H_2 mixture. Comparing the results in Figures 1 and the bottom panel in Figure 7, it is clear that a reduction in the catalytic activity of $CeO_x/Cu(111)$ is accompanied by an decrease in the concentration of Ce^{3+} on the surface of the catalyst. As the coverage of the ceria overlayer raises, the oxide film loses defects and any effect of a oxide-metal interaction diminishes making more difficult a $Ce^{4+} \rightarrow Ce^{3+}$ transformation. Theoretical calculations indicate that small aggregates of CeO_2 deposited on Cu(111) undergo partial reduction with an increase in the relative stability of Ce^{3+} with respect to Ce^{4+}.[34]

The surface chemistry of the $CeO_x/Cu(111)$ systems under reaction conditions was investigated using AP-XPS and AP-IRRAS. Figure 8 displays O 1s and C 1s XPS spectra of an as prepared $CeO_2/CuO_x/Cu(111)$ surface with ~ 0.2 ML of CeO_x (a), under 30mTorr of CO_2 at 300 K (b), with an addition of 270 mTorr of H_2 (c), and subsequent heating to 400 (d) and 500 K (e) under those conditions. In the O 1s region (left) the primary peak at 530 eV corresponds to the oxygen from CeO_x with a small contribution from the $CuO_x/Cu(111)$ substrate in the as prepare surface (a). In addition, this surface has a small concentration of OH species (531.5 eV). In the C 1s region (right) no peaks are visible except for a small contribution from surface C at 284 eV, probably coming from the dissociation of background gases. With the addition of 30mTorr of CO_2 at 300 K (b), peaks centered at 531.9 eV (O 1s) and 289.3 eV (C 1s) are now visible that can be attributed to $CO_2^{\delta-}$ species generated by the adsorption of CO_2 gas which also appears in the spectra {537.1 (O 1s) and 293eV (C 1s)}.[23] Weak features a 532.5 eV (O 1s) and 289.9 eV (C 1s) denote the presence of a small amount of formate ($HCOO^-$)[23] probably formed by reaction of CO_2 with a minor concentration of H_2 in the background gases. Subsequent addition of 270 mTorr of H_2 and heating to 400 (d) and 500 K (e) shows an increase in the features for $HCOO^-$. The small feature at 284 eV, assigned to surface C on the surface (see above), remains more or less constant through the entire experiment. A similar AP-XPS experiment for plain Cu(111) exposed to a mixture of CO_2/H_2 showed only $HCOO^-$ which is produced by direct reaction of CO_2 with adsorbed H atoms.[10,12,13,17,21] Thus, the $CO_2^{\delta-}$ appears on the surface only after the formation of the ceria-copper interface.

Experiments of AP-XPS carried out as a function of ceria coverage, reaction conditions of 30 mTorr CO_2 and 270 mTorr of H_2 at 300-500K, pointed to a maximum in the amount of adsorbed $CO_2^{\delta-}$ when the metal surface was covered 20-30% with the oxide. For a Cu(111) substrate fully covered with ceria there was formation of surface formate but not significant adsorbed $CO_2^{\delta-}$ was detected. A decrease in the coverage of adsorbed $CO_2^{\delta-}$ with increasing coverage of ceria was also observed with infrared spectroscopy. Figure 9 shows AP-IRRA spectra obtained during the exposure of low(~0.2 ML) and medium(~0.5 ML) coverages of CeO_x on Cu(111) to CO_2 (1.0 Torr) and H_2(9.0 Torr) at 500 K. These spectra show IR peaks at 1295, 1330, 1372, 1598 and 2855 cm^{-1}. The peak at 1295 cm^{-1} is assigned to carboxylate ($CO_2^{\delta-}$) [35] whereas the other features can be assigned to a formate ($HCOO^-$) species.[23] The peaks at 1330 and 1372 cm^{-1} can be assigned to symmetric OCO stretches, ν_s(OCO), whereas the peak at 1598 cm^{-1} is for the asymmetric OCO stretches ,ν_{as}(OCO), and the peak at 2855 cm^{-1} is for CH stretch,ν(CH), modes. These IR spectra show that when the coverage of ceria is increased, more formates are generated but the amount of carboxylate decreases in conjunction with the decrease in catalytic activity. Thus, it is likely that $HCOO^-$ is just a spectator and not a key intermediate for the alcohol synthesis reaction.

A comparison of the results in Figures 1, 7-9 show a correlation between the catalytic activity, the presence of Ce^{3+} sites and the generation of $CO_2^{\delta-}$ surface species. This trend supports a previous theoretical study which suggests that Ce^{3+} sites and adsorbed $CO_2^{\delta-}$ are essential in the $CO_2 \rightarrow CH_3OH$ conversion.[23] The reaction mechanism predicted by the theoretical calculations involves first the reverse water-gas shift (RWGS) reaction to generate CO and then sequential hydrogenation of this molecule: $CO \rightarrow CHO \rightarrow CH_2O \rightarrow CH_3O \rightarrow CH_3OH$. The highest predicted activation barrier is close to 15 kcal/mol and is associated with the RWGS reaction,[23] with smaller barriers for the formation of CHO, CH_2O, CH_3O and CH_3OH. In Figure 2, the copper catalysts covered 20 and 50% by ceria have an apparent activation energy near 14 kcal/mol and display much better activity than plain Cu(111) in Figure 1. In all our experiments, after systematically changing the coverage of ceria on copper, we only detected features for $HCOO^-$ and $CO_2^{\delta-}$ in AP-XPS and IRRAS. This implies that any other surface intermediates produced by the hydrogenation of CO_2 (i.e. HOCO, H_xOCO) or CO (i.e. CHO, CH_2O or CH_3O species) are short-lived in agreement with theoretical predictions.[23] Our studies with ambient-pressure photoemission and infrared spectroscopy are not enough to identify in a conclusive way the exact path for the $CO_2 \rightarrow CH_3OH$ conversion which could involve the RWGS reaction and subsequent hydrogenation of CO or direct hydrogenation of CO_2

CONCLUSION

In summary, the results in Figure 1 quite clearly indicate that the formation of a metal-oxide interface is essential for high catalytic activity in the synthesis of methanol from CO_2 hydrogenation. The nature of the oxide has a strong impact on the catalytic activity. Coverage and metal-oxide interactions affect the chemical and catalytic properties of the oxide. In the case of ceria, one has a reducible oxide in which Ce^{3+} becomes the preferred oxidation state at low coverages opening an efficient reaction channel to adsorb and transform CO_2 via a $CO_2^{\delta-}$ intermediate, instead of the more stable formate species. A comparison of the activities of CeO_x/Cu(111) and Cu/CeO_2(111), or ZnO/Cu(111) and Cu/ZnO(000$\bar{1}$), indicates that a oxide/metal configuration leads to superior catalyst. In this configuration one can optimize the participation of the oxide in the catalytic process.

AUTHOR INFORMATION

Corresponding author

*E-mail: rodrigez@bnl.gov

Notes

The authors declare no competing financial interest

ACKNOWELDGEMENTS

The research carried out in this manuscript performed at Brookhaven National Laboratory, was supported by the U.S. Department of Energy, Office of Science, Office of Basic Energy Sciences, and Catalysis Science Program under contract No. DE-SC0012704. The work performed at the Advanced Light Source is supported by the Director, Office of Science, Office of Basic Energy Sciences, of the U.S. Department of Energy under Contract No. DE-AC02-05CH11231.

Figure Captions

Figure 1 Rate for the conversion of CO_2 to methanol on Cu(111) as a function of the fraction of the metal surface covered by zinc oxide or ceria. Reaction conditions: T= 550 K, P_{H2}= 4.5 atm, P_{CO2}= 0.5 atm.

Figure 2 Part A: Arrhenius plots for the conversion of CO_2 to methanol on plain Cu(111) and on the metal surface covered 20% by nanoparticles of ZnO or Ce_2O_3. Part B: Apparent activation energies for the conversion of CO_2 to methanol on plain Cu(111) and on the metal surface covered 20 and 50% by nanoparticles of ZnO or CeO_x. Reaction conditions: P_{H2}= 4.5 atm, P_{CO2}= 0.5 atm.

Figure 3 Rates measured for the production of metanol on Cu(111),[17] Cu/ZnO(000ī),[17] ZnO/Cu(111), Cu/CeO_2(111)[23] and CeO_x/Cu(111). Reaction conditions: T= 550 K, P_{H2}= 4.5 atm, P_{CO2}= 0.5 atm.

Figure 4 Zn $2p_{3/2}$ XPS spectra obtained after performing the hydrogenation of CO_2 on ZnO/Cu(111) catalysts. T= 550 K, P_{H2}= 4.5 atm, P_{CO2}= 0.5 atm.

Figure 5 Zn $2p_{3/2}$ XPS peak position measured after reaction for a series of ZnO_x/Cu(111) catalysts. Reaction conditions: T= 550 K, P_{H2}= 4.5 atm, P_{CO2}= 0.5 atm.

Figure 6 Ce 3d XPS spectra obtained after performing the hydrogenation of CO_2 on CeO_x/Cu(111) catalysts with different coverages of ceria. Reaction conditions: T= 550 K, P_{H2}= 4.5 atm, P_{CO2}= 0.5 atm.

Figure 7 Percentage of Ce^{3+} present after reaction in a series of CeO_x/Cu(111) catalysts. The relative concentrations of Ce^{3+} and Ce^{4+} were determined by deconvoluting the corresponding Ce 3d XPS spectra.[32,33] Reaction conditions: T= 550 K, P_{H2}= 4.5 atm, P_{CO2}= 0.5 atm.

Figure 8 O 1s and C 1s XPS spectra of an as prepared CeO_2/CuO_x/Cu(111) surface with ~ 0.2 ML of CeO_x (a), under 30mTorr of CO_2 at 300 K (b), with an addition of 270 mTorr of H_2 (c), and subsequent heating to 400 (d) and 500 K (e) under those conditions.

Figure 9 AP-IRRA spectra obtained during the exposure of low (~0.2 ML) and medium (~0.5 ML) coverages of CeO_x on Cu(111) to CO_2 (1.0 Torr) and H_2 (9.0 Torr) at 500 K.

References

1. Lecomte, F.; Broutin, P.; Lebas, E. *CO_2 Capture: Technologies to Reduce Greenhouse Gas Emissions*, IFP Publications, Paris, 2010.

2. Lim, X. How to Make the Most of Carbon Dioxide. *Nature*, **2015**, *526*, 628–630.

3. Karl, T.R.; Trenberth, K.E. Modern Global Climate Change. *Science*, **2003**, *302*, 1719-1723.

4. Kondratenko, E. V.; Mul, G.; Baltrusaitis, J.; Larrazabal, G. O.; Perez-Ramirez, J. Status and Perspectives of CO_2 Conversion into Fuels and Chemicals by Catalytic, Photocatalytic and Electrocatalytic Processes. *Energy Environ. Sci.* **2013**, *6*, 3112-3115.

5. Quadrelli, A.; Centi, G.; Duplan, J.-L.; Perathoner, S. Carbon Dioxide Recycling: Emerging Large-Scale Technologies with Industrial Potential. *Chem. Sus. Chem.* **2011**, *4*, 1194-1215.

6. *Carbon Dioxide as Chemical Feedstock*, Aresta, M. (editor), Wiley-VCH, New York, 2010.

7. Service R.F., Feature: There's Too Much Carbon Dioxide in the Air. Why Not Turn it Back into Fuel? *Science* **2015**, DOI: 10.1126/science.aad1735.

8. Miguel, C.V.; Soria, M.A.; Mendes, A.; Madeira, L.M. Direct CO_2 Hydrogenation to Methane or Methanol from Post-Combustion Exhaust Streams – A Thermodynamic Study. *J. Natural Gas Science and Eng.* **2015**, *22*, 1-8.

9. Torrente-Murciano, L.; Mattia, D.; Jones, M.D.; Plucinski, P.K. Formation of Hydrocarbons Via CO_2 Hydrogenation - A Thermodynamic Study. *J. CO_2 Utilization*, **2014**, *6*, 34-39.

10. Medford, A.J.; Lausche, A.C.; Abild-Pedersen, F.; Temel, B.; Schjødt, N.C.; Nørskov, J.K.; Studt, F. Activity and Selectivity Trends in Synthesis Gas Conversion to Higher Alcohols. *Top. Catal*. **2014**, *57*, 135-142.

11. Schumann, J.; Eichelbaum, M.; Lunkenbein, T.; Thomas, N.; Álvárez-Galvan, M.C.; Schlögl, R.; Behrens, M. Promoting Strong Metal Support Interaction: Doping ZnO for Enhanced Activity of Cu/ZnO:M (M = Al, Ga, Mg) Catalysts. *ACS Catal.* **2015**, *5*, 3260-3270.

12. Rodriguez, J.A.; Liu, P.; Stacchiola, D.J.; Senanayake, S.D.; White, M.; Chen, J.G. Hydrogenation of CO_2 to Methanol: Importance of Metal–Oxide and Metal–Carbide Interfaces in the Activation of CO_2. *ACS Catal.* **2015**, *5*, 6696-6706.

13. Studt, F., Behrens, M., Kunkes, E. L., Thomas, N., Zander, S., Tarasov, A., Schumann, J., Frei, E., Varley, J. B., et al. The Mechanism of CO and CO_2 Hydrogenation to Methanol over Cu-Based Catalysts. *ChemCatChem*, **2015**, *7*, 1105–1111.

14. Lunkenbein, T.; Schumann, J.; Behrens, M.; Schlögl, R.; Willinger, M.G. Formation of a ZnO Overlayer in Industrial Cu/ZnO/Al_2O_3 Catalysts Induced by Strong Metal–Support Interactions. *Angew. Chem. Int. Ed.* **2015**, *54*, 4544-4548.

15. Slaa, J.C.; Van Ommen, J.G.; Ross, J.R.H. The Synthesis of Higher Alcohols Using Modified Cu/ZnO/Al_2O_3 Catalysts. *Catal. Today*, **1992**, *15*, 129-148.

16. Nakamura, J.; Nakamura, I.; Uchijima, T.; Kanai, Y.; Watanabe, T.; Saito, M.; Fujitani, T. A Surface Science Investigation of Methanol Synthesis over a Zn-Deposited Polycrystalline Cu Surface. *J. Catal.* **1996**, *160*, 65-75.

17. Yang, Y.; Evans, J.; Rodriguez, J.A.; White, M.G.; Liu, P. Fundamental studies of methanol synthesis from CO_2 hydrogenation on Cu(111), Cu clusters, and Cu/ZnO(0001). *Phys. Chem. Chem. Phys*. **2010**, *12*, 9909-9917.

18. Yoshihara, J.; Campbell, C.T. Methanol Synthesis and Reverse Water–Gas Shift Kinetics over Cu(110) Model Catalysts: Structural Sensitivity. *J. Catal*. **1996**, *161*, 776-783.

19. Rasmussen, P.B.; Holmblad, P.M.; Askgaard, T.; Ovesen, C.V.; Stoltze, P.; Nørskov, J.K.; Chorkendorff, I. Methanol Synthesis on Cu(100) from a Binary Gas Mixture of CO_2 and H_2. *Catal. Lett*. **1994**, *26*, 373-379.

20. Szanyi, J.; Goodman, D.W. Methanol Synthesis on a Cu(100) Catalyst. *Catal. Lett.* **1991**, *10*, 383-390.

21. Grabow, L.C.; Mavrikakis, M. Mechanism of Methanol Synthesis on Cu through CO_2 and CO Hydrogenation. *ACS Catal*. **2011**, *1*, 365-384.

22. Kandemir, T.; Kasatkin, I.; Girgsdies, F.; Zander, S.; Kühl, S.; Tovar, M.; Schlögl, R.; Behrens, M., Microstructural and Defect Analysis of Metal Nanoparticles in Functional Catalysts by Diffraction and Electron Microscopy: The Cu/ZnO Catalyst for Methanol Synthesis. *Top. Catal.* **2014**, *57*, 188–206.

23. Graciani, J.; Mudiyanselage, K.; Xu, F.; Baber, A. E.; Evans, J.; Senanayake, S. D.; Stacchiola, D. J.; Liu, P.; Hrbek, J.; Sanz, J. F.; Rodriguez, J. A. Highly Active Copper-Ceria-Titania Catalysts for Methanol Synthesis from CO_2. *Science* **2014**, *345*, 546-551.

24. Ogletree, D.F.; Bluhm, H.; Lebedev, G.; Fadley, C.S.; Hussain, Z.; Salmeron, M. A Differentially Pumped Electrostatic Lens System for Photoemission Studies in the Millibar Range. *Rev. Sci. Instrum.* **2002**, *73*, 3872.

25. Hrbek, J.; Hoffmann, F.M.; Park, J.B.; Liu, P.; Stacchiola, D.; Hoo, Y.S.; Ma, S.; Nambu, A.; Rodriguez J.A.; and White, M.G.; Adsorbate-Driven Morphological Changes of a Gold Surface at Low Temperatures. *J. Am. Chem. Soc.*, **2008**, *130*, 17272-17273.

26. Campbell, C.T. Ultrathin Metal Films and Particles on Oxide Surfaces: Structural, Electronic and Chemisorptive Properties. *Surf. Sci. Reports*, **1997**, *27*, 1-111.

27. Henry, C. Surface Studies of Supported Model Catalysts. *Surf. Sci. Reports*, **1998**, *31*, 231-325.

28. Vidal, A.; Liu, P. Density Functional Study of Water-Gas Shift Reaction on M_3O_{3x}/Cu(111). *Phys. Chem. Chem. Phys.* **2012**, *14*, 16626-16632.

29. Pacchioni, G.; Freund, H.J. Electron Transfer at Oxide Surfaces. The MgO Paradigm: from Defects to Ultrathin Films. *Chem. Rev.* **2013**, *113*, 4035–4072.

30. Campbell, C.T.; Daube, K.A.; White, J.M. Cu/ZnO(0001) and ZnOx/Cu(111): Model catalysts for Methanol Synthesis. *Surf. Sci.* **1987**, *182*, 458-476.

31. Vohs, J.M.; Barteau, M.A. Spectroscopic Characterization of Surface Formates Produced via Reaction of HCOOH and $HCOOCH_3$ on the (0001) Surface of Zinc Oxide. *Surf. Sci.* **1986**, *176*, 91-114.

32. Pfau, A.; Schierbaum, K.D. The Electronic Structure of Stoichiometric and Reduced CeO_2 Surfaces: An XPS, UPS and HREELS Study. *Surf. Sci.* **1994**, *321*, 71-80.

33. Rodriguez, J.A.; Ma, S.; Liu, P.; Hrbek, J.; Evans, J.; Pérez, M. Activity of CeO_x and TiO_x Nanoparticles Grown on Au(111) in the Water–Gas Shift Reaction. *Science*, **2007**, *318*, 1757-1760.

34. Graciani, J.; Vidal, A.B.; Rodriguez, J.A.; Sanz, J.F. Unraveling the Nature of the Oxide–Metal Interaction in Ceria-Based Noble Metal Inverse Catalysts. *J. Phys. Chem. C*, **2014**, *118*, 26931-26938.

35. Mudiyanselage, K.; Senanayake, S.D.; Feria, L.; Kundu, S.; Baber, A.E.; Graciani, J.; Vidal, A.B.; Agnoli, S.; Evans, J.; Chang, R.; et al.; Importance of the Metal–Oxide Interface in Catalysis: In Situ Studies of the Water–Gas Shift Reaction by Ambient-Pressure X-ray Photoelectron Spectroscopy. *Angew. Chem. Int. Ed.*, **2013**, *52*, 5101-5105.

TOC

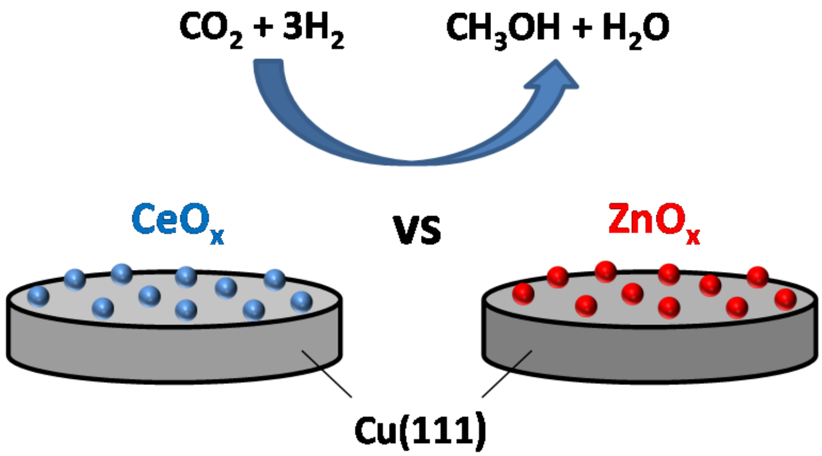

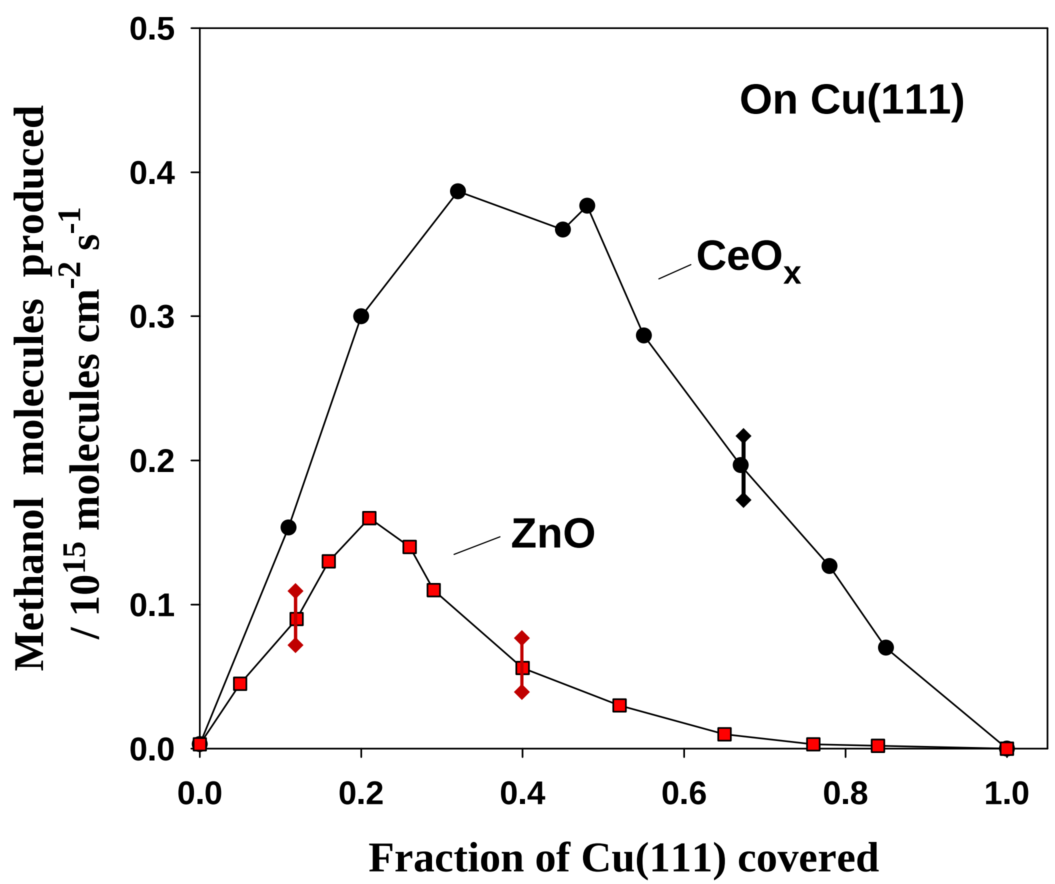

On Cu(111)
CeO$_x$
ZnO
Methanol molecules produced / 10^{15} molecules cm^{-2} s^{-1}
Fraction of Cu(111) covered
0.0
0.1
0.2
0.3
0.4
0.5
0.0
0.2
0.4
0.6
0.8
1.0

Fig 1

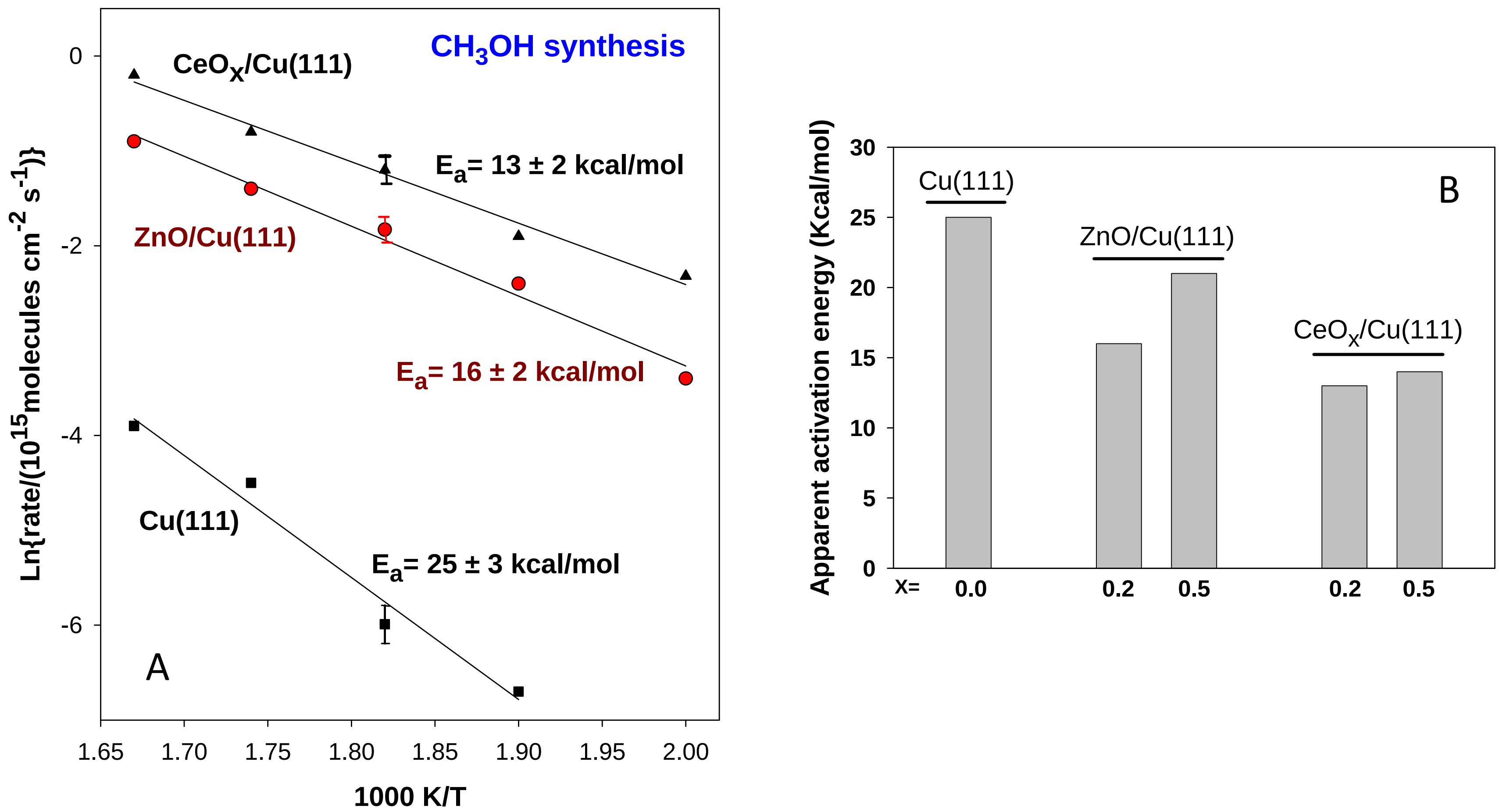

CH3OH synthesis
CeOx/Cu(111)
Ea= 13 ± 2 kcal/mol
ZnO/Cu(111)
Ea= 16 ± 2 kcal/mol
Cu(111)
Ea= 25 ± 3 kcal/mol
A
Ln{rate/(10^15 molecules cm^-2 s^-1)}
0
-2
-4
-6
1.65
1.70
1.75
1.80
1.85
1.90
1.95
2.00
1000 K/T
Apparent activation energy (Kcal/mol)
0
5
10
15
20
25
30
Cu(111)
ZnO/Cu(111)
CeOx/Cu(111)
B
X=
0.0
0.2
0.5
0.2
0.5

Fig 2

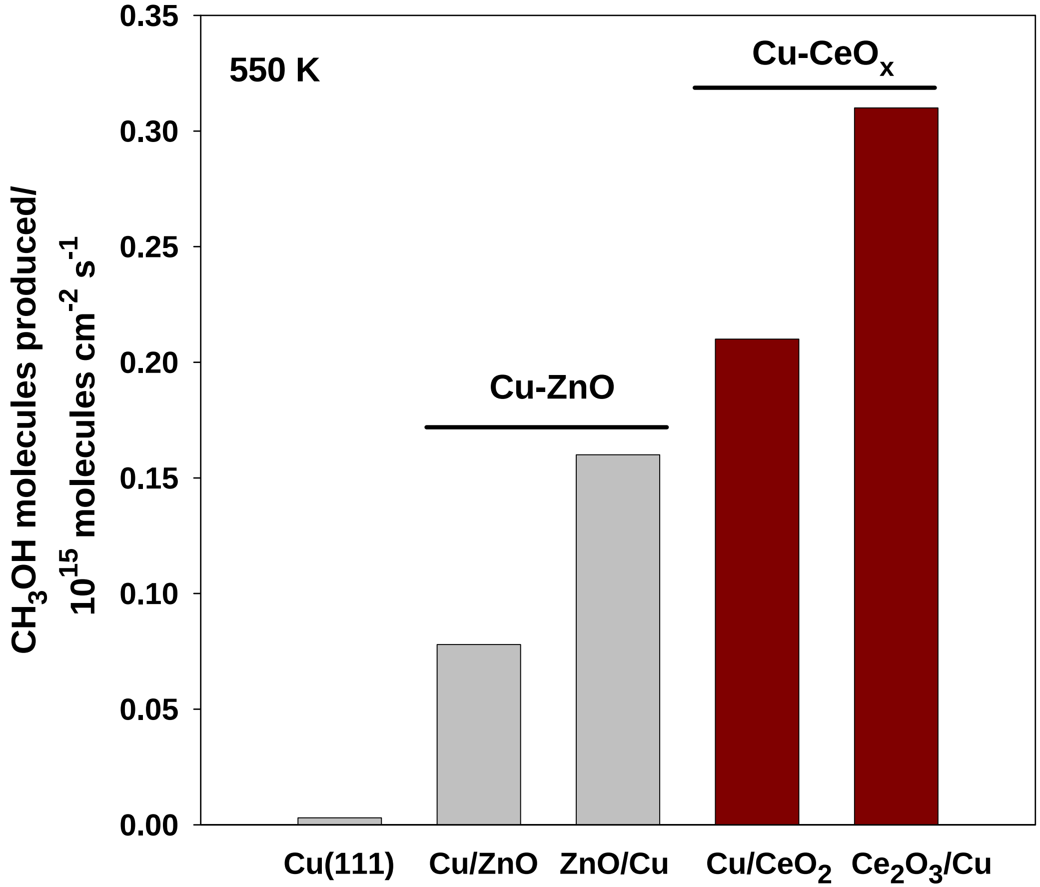

0.35
0.30
0.25
0.20
0.15
0.10
0.05
0.00
550 K
Cu-ZnO
Cu-CeO$_x$
CH$_3$OH molecules produced/
10^{15} molecules cm^{-2} s^{-1}
Cu(111)
Cu/ZnO
ZnO/Cu
Cu/CeO$_2$
Ce$_2$O$_3$/Cu

Fig 3

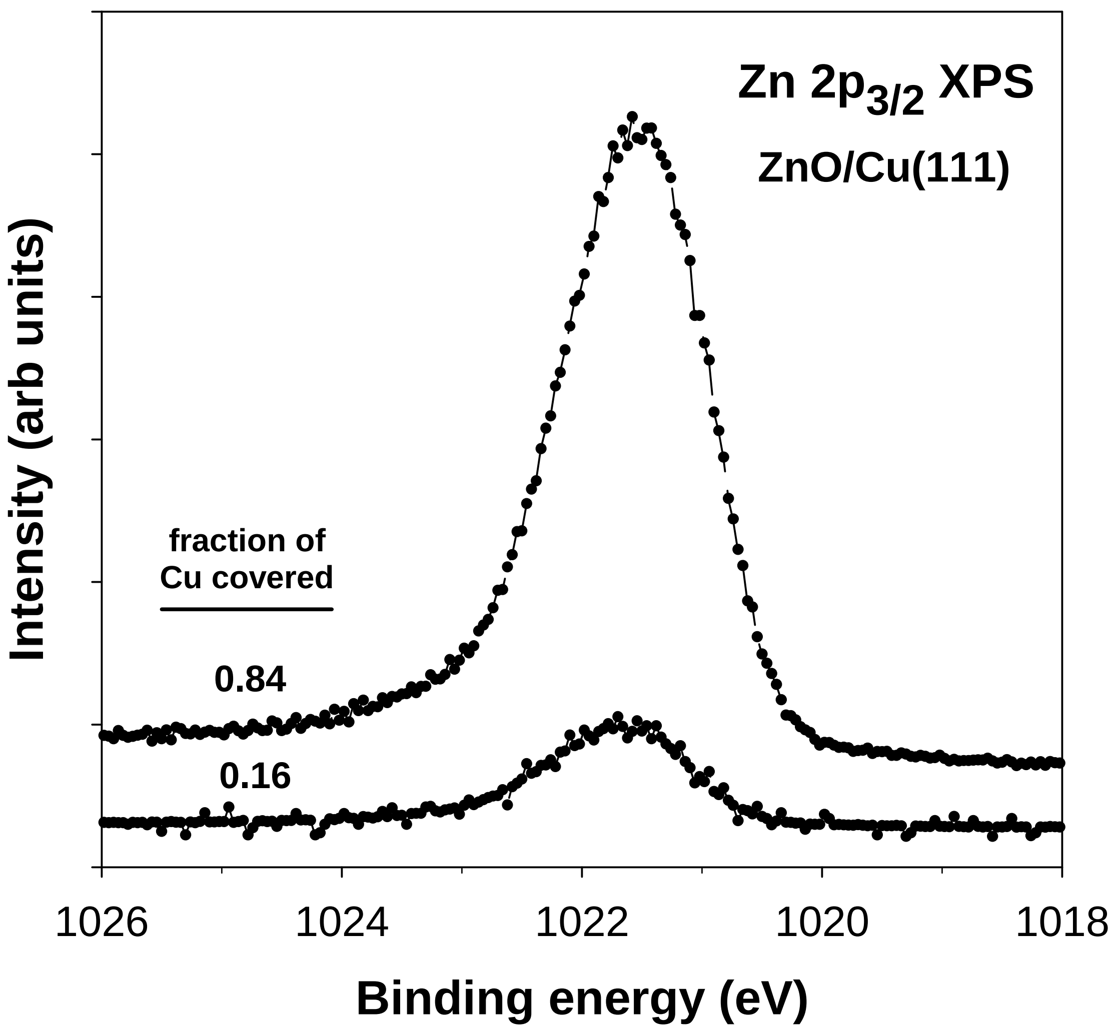

Zn 2p3/2 XPS
ZnO/Cu(111)
fraction of
Cu covered
0.84
0.16
Intensity (arb units)
1026
1024
1022
1020
1018
Binding energy (eV)

Fig 4

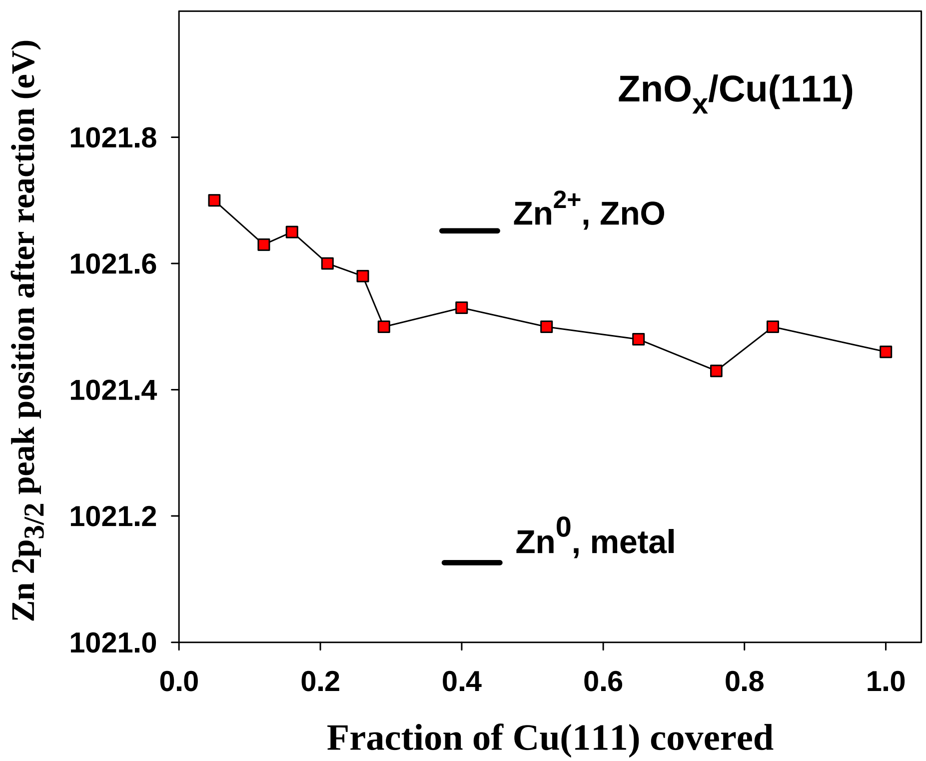
ZnO$_x$/Cu(111)
Zn^{2+}, ZnO
Zn^0, metal
1021.8
1021.6
1021.4
1021.2
1021.0
0.0
0.2
0.4
0.6
0.8
1.0
Zn 2p$_{3/2}$ peak position after reaction (eV)
Fraction of Cu(111) covered

Fig 5

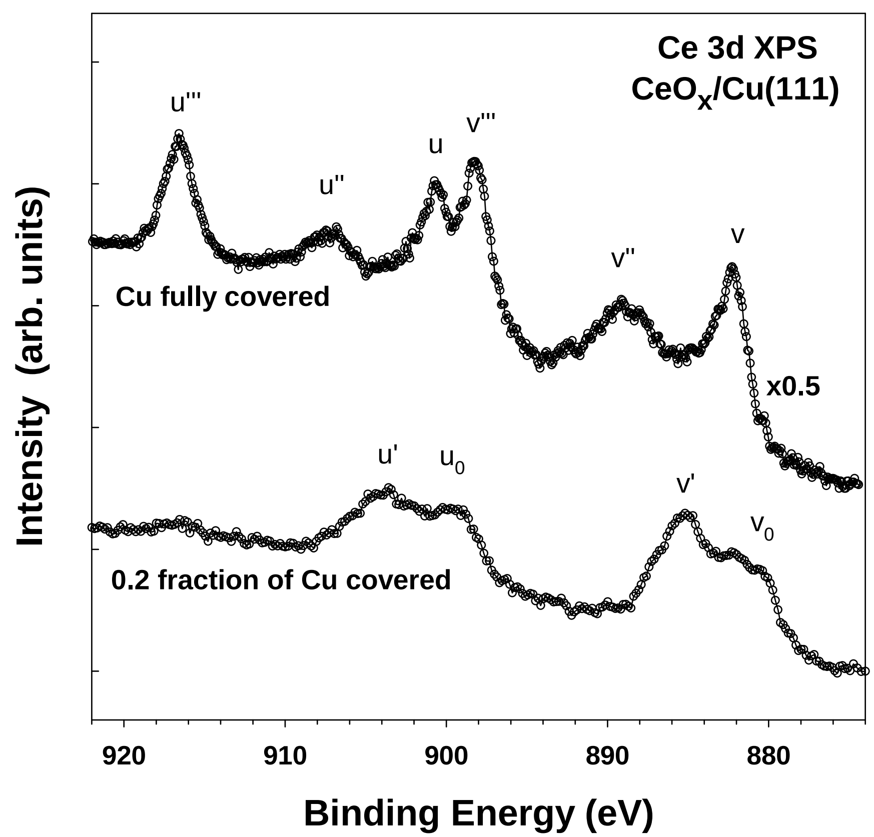
Ce 3d XPS
CeO$_x$/Cu(111)
u'''
u''
u
v'''
v''
v
Cu fully covered
x0.5
u'
u$_0$
v'
v$_0$
0.2 fraction of Cu covered
Intensity (arb. units)
920
910
900
890
880
Binding Energy (eV)

Fig 6

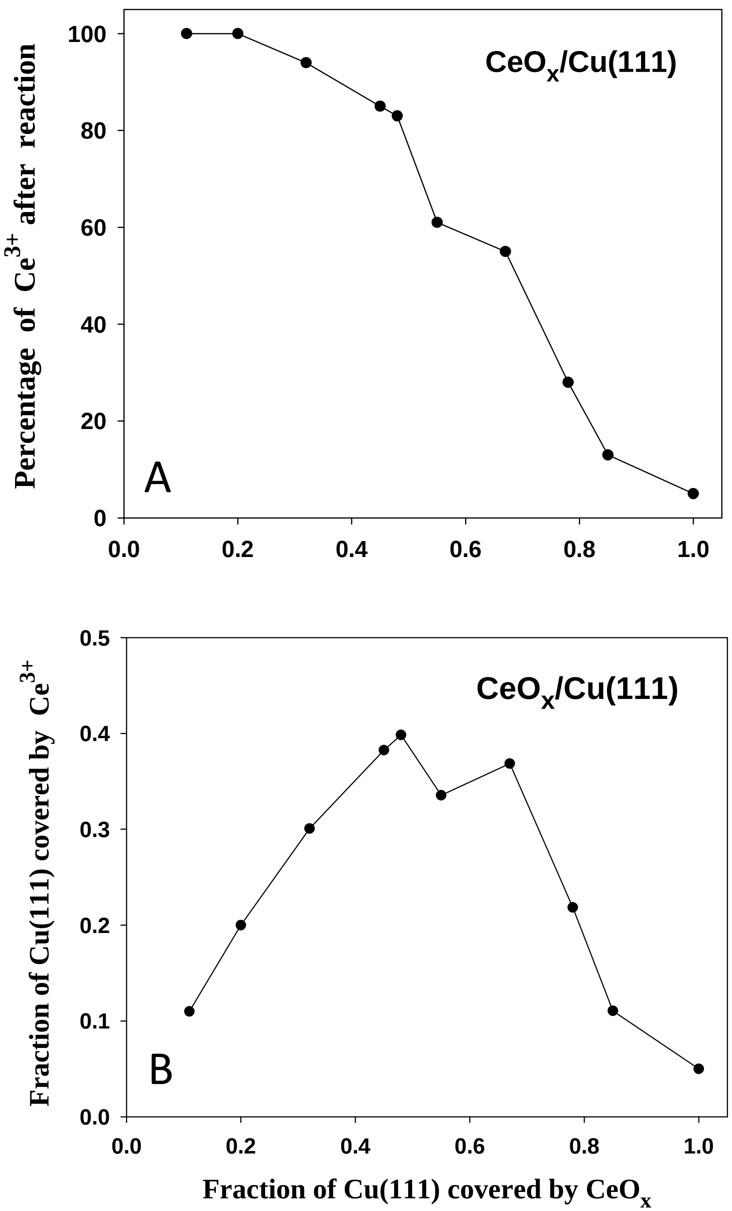
CeO$_x$/Cu(111)
A
Percentage of Ce^{3+} after reaction
100
80
60
40
20
0
0.0
0.2
0.4
0.6
0.8
1.0
CeO$_x$/Cu(111)
B
Fraction of Cu(111) covered by Ce^{3+}
0.5
0.4
0.3
0.2
0.1
0.0
Fraction of Cu(111) covered by CeO$_x$

Fig 7

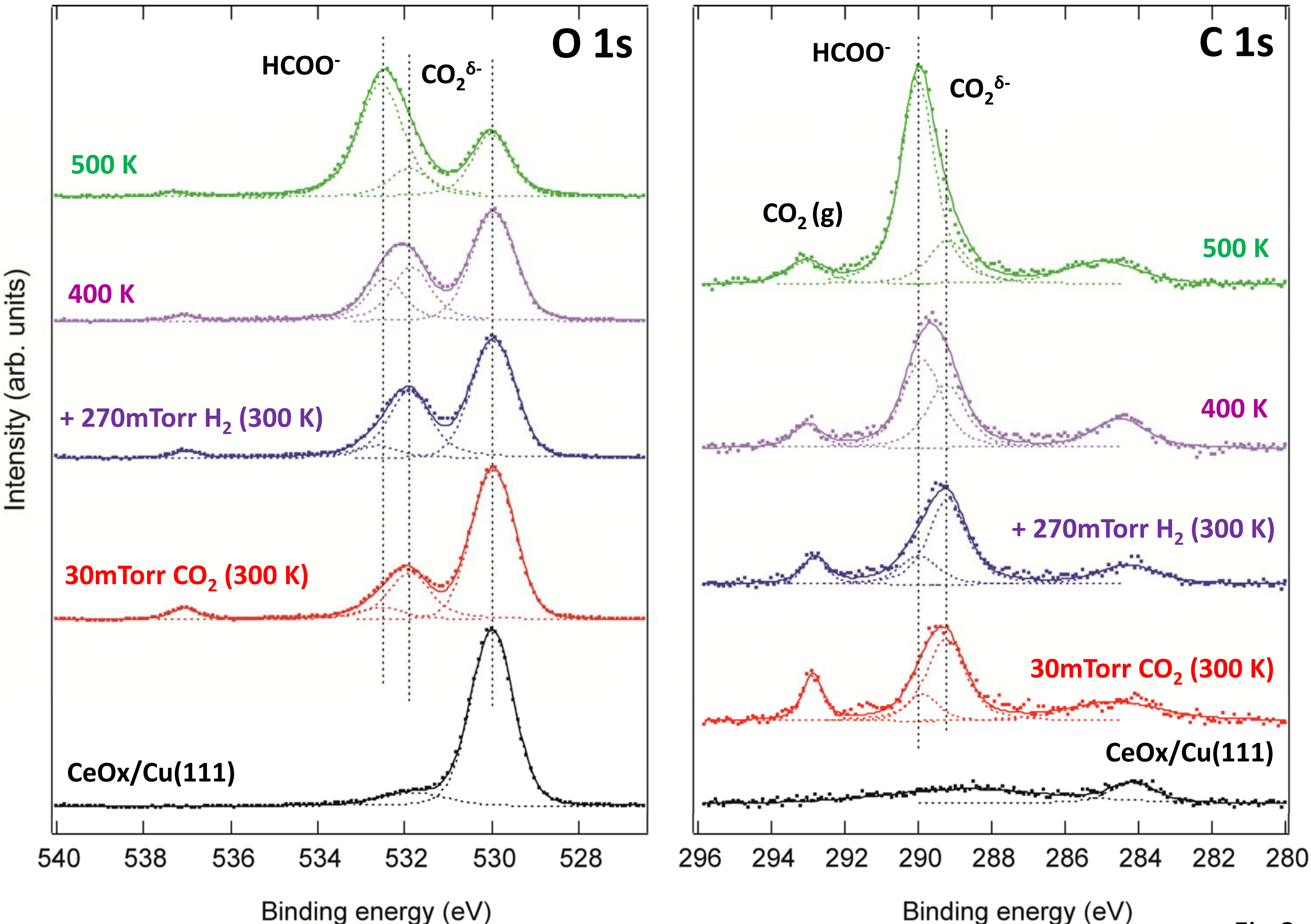

O 1s
HCOO-
$CO_2^{\delta-}$
500 K
400 K
+ 270mTorr H_2 (300 K)
30mTorr CO_2 (300 K)
CeOx/Cu(111)
Intensity (arb. units)
540
538
536
534
532
530
528
Binding energy (eV)
C 1s
HCOO-
$CO_2^{\delta-}$
CO_2 (g)
500 K
400 K
+ 270mTorr H_2 (300 K)
30mTorr CO_2 (300 K)
CeOx/Cu(111)
296
294
292
290
288
286
284
282
280
Binding energy (eV)

Fig 8

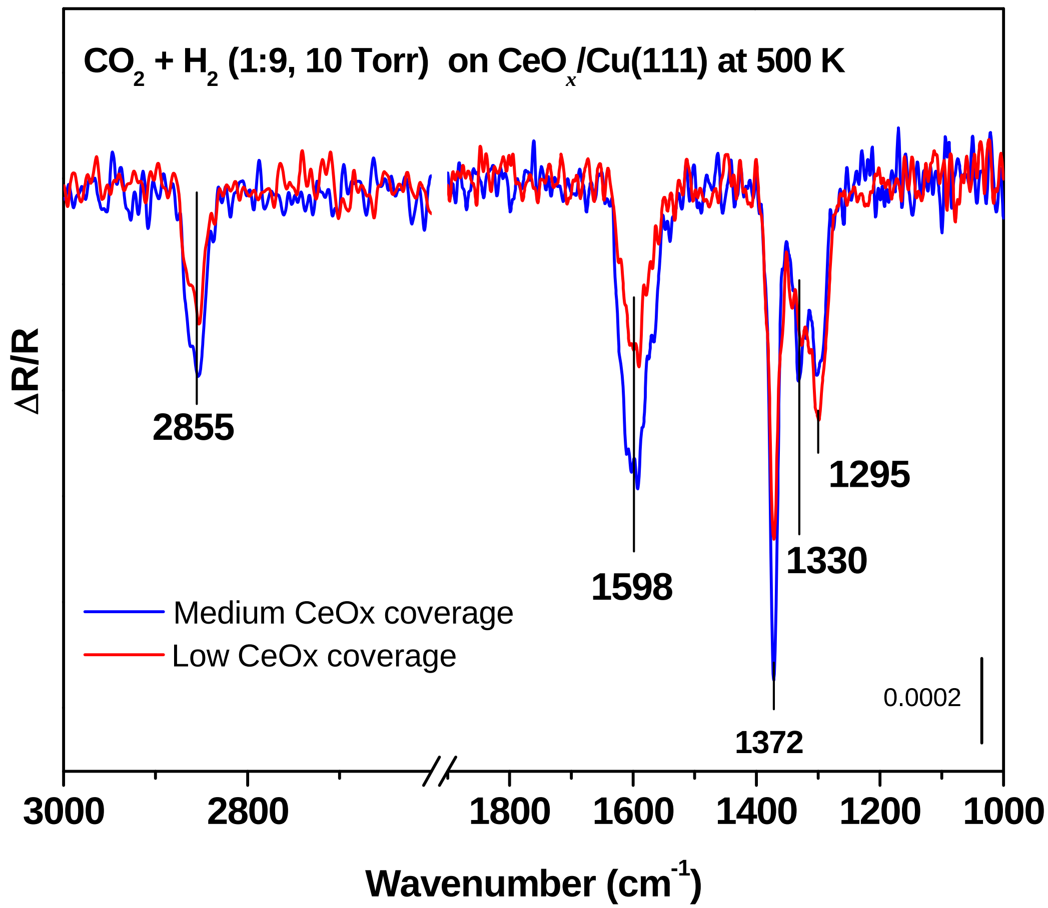

CO2 + H2 (1:9, 10 Torr) on CeOx/Cu(111) at 500 K
ΔR/R
2855
1598
1372
1330
1295
Medium CeOx coverage
Low CeOx coverage
0.0002
3000
2800
1800
1600
1400
1200
1000
Wavenumber (cm-1)

Fig 9